THE JOURNAL OF PHYSICAL CHEMISTRY B

Article

pubs.acs.org/JPCB

Ordered Assemblies of Triangular-Shaped Molecules with Strongly Interacting Vertices: Phase Diagrams for Honeycomb and Zigzag Structures on Triangular Lattice

T. Misiūnas and E. E. Tornau*

Semiconductor Physics Institute, Center for Physical Sciences and Technology, A. Goštauto 11, LT-01108, Vilnius, Lithuania

ABSTRACT: The model for ordering of triangular-shaped molecules with strongly interacting vertices is proposed and solved by the Monte Carlo method. The model accounts for three main intermolecular interactions and three states (two main orientations and a vacancy state) of a molecule on triangular lattice, the situation which is encountered in self-assembly of TMA molecules characterized by strongly directional H-bonding. Distinguishing the main "tip-to-tip" interaction, we calculate the phase diagrams for the honeycomb and frustrated honeycomb structures and demonstrate how these structures shrink and vanish with gradual increase of two other ("side-to-side" and "tip-to-side") interactions. We study the effect of frustration on the phase diagram, since the frustrated phase is obtained at the Ising limit of the model. We also demonstrate how the inclusion of longer-range interactions leads to substitution of the frustrated phase by the zigzag structure. Finally, we obtain the phase diagram with two experimentally found TMA structures (honeycomb and zigzag) and discuss the conditions of their existence by comparison with the experimental results.

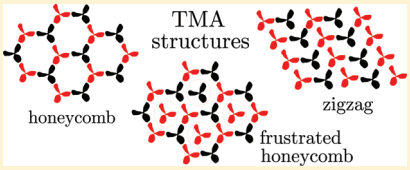

I. INTRODUCTION

Development of methods for direct investigation, such as STM, provided an abundance of data on self-organization of molecules and molecular blocks. Different, sometimes quite exotic, ordered nanostructures assembled by Coulomb, van der Waals, and H-bond couplings were found and studied,[1−11] and different bonding schemes were determined and analyzed.[6,12−15]

The formation of long-range two-dimensional molecular networks is controlled by many important factors. As key factors, the intermolecular and adsorbate−substrate interactions,[5,6,13,10,16,15] the geometry and symmetry of assembling molecules,[7,8,10,12,13] the selective coupling of molecules to preferential adsorption sites of the surface,[2,8,17] and the effects of temperature and solvent[8,12,13] might be mentioned.

The molecular networks built by molecules coupled by highly directional forces, H-bonds in particular, comprise a specific group of such self-assemblies. Recently, very interesting reports of two-dimensional molecular networks, composed of trimesic acid (TMA),[8,10,12,15,18−23] 1,3,5-benzenetribenzoic acid (BTB),[24,16] PTCDA−melamine system,[17,25,26] antraquinone on Cu(111),[7] star-shaped oligofluorene end-capped with carboxylic groups (StOF−COOH3),[27] and some other similar[9,28] molecules, were published.

Specifically, triangular-shaped TMA and BTB are relatively simple organic molecules with a strict geometrical three-leg (trimeric) form originating from the central phenyl ring. The ordering of these molecules is controlled by highly directional H-bonding (both dimeric and trimeric) at the vertices of the triangle. Both molecules are well-known building blocks for construction of the porous honeycomb lattice which is suitable for incorporation, storage, and manipulation of some small guest molecules, e.g., C60.[8] Some other polymorph structures composed of these molecules are also characterized as very strongly and nicely ordered formations.[10,12,18,21] It should be noted that the honeycomb and some other polymorph structures formed of these molecules might be obtained either at high vacuum conditions, e.g., on Au(111)[19−21] and Cu(100),[22] or on solid/liquid interface by tuning an appropriate concentration of solvent fatty acids on highly ordered pyrolytic graphite (HOPG).[8,10,12,16,18,23]

Two-dimensional ordered molecular networks and the honeycomb structure in particular can be assembled (usually on hexagonal substrates) also by different types of triangular-shaped molecules. As some examples, we can mention the ordering of SubPc molecules on Ag(111)[29,30] or discotic liquid crystals of symmetrically alkoxy-substituted triphenylenes on HOPG.[31,32] But ordering of both SubPc and liquid crystal is governed by less direct forces than those of the TMA and BTB, and SubPc does not form such perfect honeycomb order as that found in TMA and BTB, where the vertices of the triangle are very active interaction centers (as they are, e.g., in the Andelman and de Gennes tripod amphiphile model[33,34] for Langmuir monolayers).

The density functional theory (DFT)[10,35] and molecular mechanics (MM)[15,16] calculations were used to obtain the formation energies of molecular assemblies and intermolecular interactions of TMA and BTB molecules. In general, ab initio methods are extremely popular and successfully describe small groups of molecules or simple periodic molecular structures. They correctly predict the ground state structure but are not used to determine the stability limits of the ordered phase when the aim is to find the temperature at which the ordered

Received: June 30, 2011
Revised: December 9, 2011
Published: January 6, 2012

molecular structure loses its long-range order. Then, as one of the options, the Monte Carlo (MC) method might be employed.

It should be noted that MC simulations of two-dimensional self-assemblies of organic molecules are still rather scarce. The arising problems comprise (1) large size of molecules and long intermolecular distances which require intricate scaling of substrate lattice; (2) complicated interaction mechanisms of large molecules involving multipole interactions instead of simple interactions of point particles or centers of mass; (3) subtle balance between scaled short-range and indirect (mostly, via substrate) long-range interactions of dipole−dipole or elastic origin; (4) existence of infinite exclusion of interactions due to large molecular size, etc.

Nevertheless, certain statistical models, which were used earlier to describe similar ordering schemes in liquid crystals,[36] polymers,[37] proteins,[38] or colloid particles,[39,40] in a modified form are successfully transferred for description of self-assembling molecular systems. These models are more complicated versions of the two-state models (Ising, lattice−gas, binary alloy) as well as extensions of these models to larger number of states (Potts[41] and Blume−Emery−Griffits[42,43]) due to multiorientational behavior of the ordering molecular species. In all these models the atomistic detail is usually neglected; i.e., the molecules are represented by rather simple geometrical shapes and orientations on a lattice and governed by defined interaction rules. These simulations allow to predict the phase diagrams and growth dynamics of different self-assembled molecular structures.

Here we would like to mention some of the most characteristic recent models and MC simulations of H-bonded molecular networks. The combined study in the PTCDA−melamine system[25] of STM images of H-bonded ordered molecular monolayers and MC simulations of their structural stability allowed to obtain the binding energies of different molecular structures. The model[26] of the honeycomb and compact phases formation in this system resulted in calculation of the phase diagram. Another phase diagram, which successfully reproduces the phases encountered in real systems, was obtained by MC simulation of the semiquantitative model[44] assuming planar molecules as a set of hexagonal tiles capable of complementary H-bonding. The kinetic MC simulation[45] mimicked the self-assembly of hexagonally shaped molecules, such as cyanuric acid and melamine, and their island formation and growth dynamics. A recent lattice−gas model[46] with short and long-range interactions was proposed and solved to explain the spontaneous formation of the honeycomb phase of antraquinone molecules on Cu(111).

Some important results were obtained in simulations when molecules are not initially tethered to the sites of underlying lattice. In effort to predict the self-assembly and time evolution of different structures of benzenedicarboxylic acids (TPA, IPA, and PA), a combined molecular dynamics (MD) and MC study[47] was performed, and the values of dimer and trimer H-bond energies obtained by DFT calculations were used as input parameters. In a combined MM, DFT, and MC study,[48] the emerging patterns of second-generation Fréchet dendrons were analyzed: the atomic positions and effective interaction potentials obtained from energy-minimized MM calculations were used as an input in the electronic structure DFT modeling and interaction-site MC modeling which were further applied to explore the ground state predictability of resulting structures. The kinetic MC simulation[49] of growth dynamics and final packing structures of thiophene-based aromatic molecules on Au(111) was performed using molecule−molecule and substrate−molecule interactions obtained by ab initio calculation. In addition, the MD technique was used to examine various polymorphs of obtained molecular structures. Similarly, the modeling by kinetic MC of the thin film growth of small organic molecules (represented as a two-site dimer) was performed in ref 50. Thus, the MC method (or kinetic MC method for simulation of structure growth) is a powerful tool to predict design rules, morphology regimes, and structure growth kinetics, especially when it is combined with the ab initio and MD techniques.

In this paper we develop and apply the statistical model for ordering of triangular molecules with strongly interacting vertices. We take into account three main mutual orientations of a pair of interacting molecules encountered in experiments. The model might be used for symmetrical trimers and tripod-type molecules, but our closest example is the ordering of the TMA molecules. Our model is restricted to pair interaction schemes only. In section 2 we introduce the nearest neighbor (NN) model and method of MC simulation. In section 3 we present the results obtained for this model, namely, the phase diagrams in which the main role is played by the honeycomb phase. We also discuss its neighbor phases and demonstrate the effect of frustration and supporting interaction constants on a region of the honeycomb phase existence. In section 4 we show how accounting for longer-range interactions leads to substitution of the frustrated phase by the zigzag structure experimentally encountered during TMA molecules ordering at close packing. Finally, we compare our results with some other results obtained studying TMA molecules ordering.

II. NEAREST NEIGHBOR MODEL

A. Binding Schemes, Interactions and Bond Vectors.

The TMA molecule is comprised of three carboxyl acid groups ordered in a planar triangular arrangement around the central phenyl ring. The carboxyl groups allow the molecule to act as a hydrogen-bonding unit and create different molecular structures.

When TMA molecules are deposited onto the hexagonal-type surface (HOPG, Au(111), etc.), the hydrogen bonding dominates intermolecular interaction and three main mutual short-range alignments of molecules are experimentally distinguished. The alignment, in which the acid group at the tip of a TMA molecule points to the "tip" of a neighbor (ε_1 in Figure 1a), is the most typical one caused by dimeric hydrogen bonding between the acid groups. This type of bonding is the basic element of the honeycomb phase in which every molecule in one state is connected by "tip-to-tip" bonds to three neighboring molecules in another state (see Figure 1c, above). In addition, two other possible H-bonding modes with "side-to-side" (ε_2) and "tip-to-side" (ε_3) attachments are also observed both at low[14] and high[15] TMA density. It should be noted that here in Figure 1 we neglect for simplicity the fact that ε_2 interaction in reality is a little bit more deformed to accommodate the best H-bonding.[14]

Here we propose the three-state model with three types of molecule pair interactions shown in Figure 1a. Discerning the orientations which constitute the basic element of experimentally obtained structures, it is possible to determine two main orientations of TMA molecule (Figure 1b) and assign them to the sites of triangular lattice (Figure 1c). Thus, in our model we assume that the self-assembly process of triangular molecules is governed by their movement along the sites of triangular lattice and rotation by 60° between these two possible

dx.doi.org/10.1021/jp206181p | J. Phys. Chem. B 2012, 116, 2472−2482

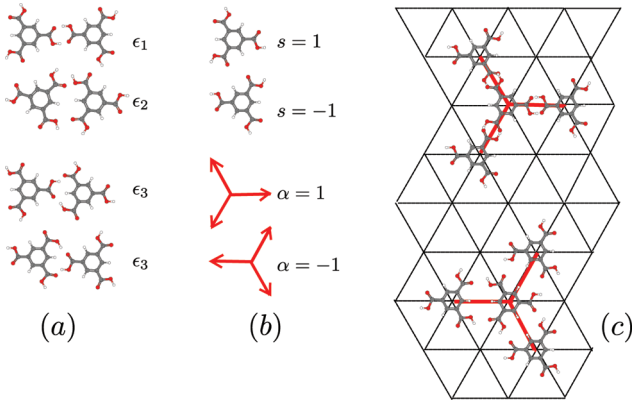

Figure 1. (a) Schematic representation of possible pair interactions (from top to bottom): tip-to-tip (energy ε_1), side-to-side (ε_2), and tip-to-side (ε_3). (b) Orientations (states $s_i = \pm 1$) of TMA molecule and bond vectors ($\alpha = \pm 1$) shown by solid gray (red in electronic version) lines with arrows. (c) Illustration of different interaction energies of TMA molecule in a state $s = 1$ surrounded in NN positions of triangular lattice by three molecules in a state $s = -1$: above (bond vector orientation $\alpha = 1$) the interaction energy is $-3\varepsilon_1$, below ($\alpha = -1$) it is $-3\varepsilon_2$. Gray (red in electronic version) lines mark bond vector orientation.

orientations (states) in the site. We also account for the possibility of molecular vacancy state, i.e., the three-state variable is $s_i = 0, \pm 1$. To obtain the honeycomb phase binded by ε_1 only, we have to discriminate between the tip-to-tip and side-to-side orderings, i.e., the inequivalent or antiferromagnetic layouts of Figure 1c (see the comparison with magnetism models in the Appendix). To do this, we introduce the concept of pair energies which are dependent on a bond vector α, i.e., the direction of the connecting lattice vector. Both orientations of the bond vector and their correspondence to two orientational states of the TMA molecule are demonstrated in Figure 1b. This idea was first used to describe the Ising-type interaction of trimer colloid particles.[39] Our "diluted" Hamiltonian has the following form

$$\mathcal{H} = -\sum_{\alpha}\sum_{\{i,j\}_\alpha} v(s_i, s_j; \alpha) + \mu \sum_i s_i^2 \qquad (1)$$

where the interactions $v(s_i, s_j; \alpha)$ are defined by bond vector orientations $\alpha = \pm 1$ and μ is the chemical potential. Locally, the interactions $v(s_i, s_j; 1)$ and $v(s_i, s_j; -1)$ are selected from energy functionals

$s_i \backslash s_j$	1	-1
1	ε_3	ε_1
-1	ε_2	ε_3

and

$s_i \backslash s_j$	1	-1
1	ε_3	ε_2
-1	ε_1	ε_3

respectively.

We also assume that the interaction of a molecule in any state with a vacant site ($s_i = 0$ state) is zero. Note also that reversing the order of the lattice sites in eq 1 leads to inversion of the bond vector $\{i, j\}_\alpha = \{j, i\}_{-\alpha}$.

We attached the site of an underlying lattice to the center of the molecule mostly for computational convenience: the Monte Carlo simulation of the lattice model requires less computational resources than the model with molecules not tethered to the sites of particular lattice and governed by distance-dependent intermolecular interactions. The choice of triangular lattice for modeling of threefold molecules is motivated by two reasons: typical underlying lattice in experiments has similar symmetry (either hexagonal or honeycomb) and the fact that the majority of experimentally found molecular assemblies demonstrate the features of hexagonal ordering. It should be noted, though, that in general the influence of a substrate is rather weak for molecular ordering, but the tendency of triangular-shaped molecules to hexagonal type of order is very strong (see, e.g., refs 29, 30, and 44), and therefore it is reasonable to approximate the system as a lattice system with hexagonal or triangular structure.

As is seen in eq 1 and Figure 1c, we restrict $v(s_i, s_j; \alpha)$ to NN interactions; i.e., as the NN distance we assume the intermolecular distance in a honeycomb phase of TMA (9.5−9.8 Å[9,12,21,20]) or BTB (18.5 Å[13]) molecules, and the NN interaction ε_1 would roughly correspond to dimeric H-bond interaction of two molecules taken from DFT[10] or pseudopotential[15] calculations. In "real" experiment there are obviously more sites for TMA molecules diffusion and ordering than this simple model allows, but most of these sites are usually forbidden due to the large size of the molecule.

B. Method of Calculation and Thermodynamic Functions. In Monte Carlo simulation of the phase transitions between the molecular structures, two types of dynamics might be used to obtain the thermodynamic functions. Using the so-called Glauber dynamics, the chemical potential μ is fixed and the lattice is filled with a corresponding concentration of molecules c; i.e., the sites of triangular lattice are completely occupied with molecules in states +1, −1, and vacancies (state 0). At first the molecule is chosen randomly and its initial NN energy E_i is calculated. Then the initial state of that molecule is changed (with equal probability) to one of two remaining states, and the final energy E_f is calculated. As a result, the energy difference $\Delta E = E_f - E_i$ is obtained. Then the Metropolis procedure[51] is performed: the new state is accepted, if $\Delta E < 0$, or accepted with the probability $\sim \exp(-\Delta E/kT)$, if $\Delta E > 0$. Using this type of dynamics the molecular concentration is changed at fixed chemical potential. Using the so-called Kawasaki dynamics the concentration is fixed, and the molecule chosen randomly makes jumps from one site to another with the probability $\exp(-\Delta E/kT)$. In our simulation here we used Glauber dynamics which is very convenient for description of statical properties of ordering systems and much less time-consuming than the Kawasaki one.

For calculations we used the triangular lattice of 36 × 30 sites and performed 10^5 MCs for each value of T and μ. The results for larger lattices showed that this lattice size is sufficient for our calculations. We calculated the dependences of thermodynamic functions (average energy $E = \langle \mathcal{H} \rangle$, specific heat $C_v = (1/k_B T^2)(\langle \mathcal{H}^2 \rangle - \langle \mathcal{H} \rangle^2)$, order parameter of the honeycomb phase, and susceptibility χ) which characterize the phase transition points at different values of temperature and chemical potential. The order parameter of the honeycomb phase has the usual form for the three-sublattice model on triangular lattice

$$\eta = \frac{3}{2} \sum_{\alpha \neq \beta \neq \gamma} \left(\frac{N_\alpha^A + N_\beta^B + N_\gamma^C}{N} - \frac{1}{3} \right) \qquad (2)$$

where A, B, C denote three sublattices and $N_{\alpha,\beta,\gamma}^{A,B,C}/N$ mean their occupancy by molecules or vacancies in states $\alpha, \beta, \gamma = \pm 1$ or 0. Thus in a disordered phase all nine $N_{\pm 1,0}^{A,B,C}/N$ are equal to 1/9 and $\eta = 0$, and in a pure honeycomb phase only $N_{+1}^A/N = N_{-1}^B/N = N_0^C/N = 1/3$ have nonzero values and $\eta = 1$.

Here we briefly describe how the phase diagrams of the model 1, presented in the next the section, were obtained. First, we performed the calculation of the ground state ($T = 0$) energies of possible ordered structures to determine those phases which have the lowest energy and might be expected on

dx.doi.org/10.1021/jp206181p | J. Phys. Chem. B 2012, 116, 2472−2482

the phase diagram. Second, for different values of temperature we calculated the $c(\mu)$ dependences. The steps in this plot at some values of concentration demonstrate the stoichiometry of pure phases which might exist on the phase diagram. It also shows the transitions between the phases of different concentration. In our model some of these transitions are of the first order (discontinuity in $c(\mu)$ dependence). It should be noted that the discontinuities are frequently encountered in antiferromagnetic models to which our model might be reduced. The discontinuities are caused by phase separation which leads to formation of two-phase regions (sometimes called mixed phases). Consequently, one value of the chemical potential μ_c corresponds to two values of concentration c_1 and c_2 between the stable phases 1 ($\mu > \mu_c$, $c \le c_1$) and 2 ($\mu < \mu_c$, $c \ge c_2$). In the phase (c, T) diagram this discontinuity corresponds to a two-phase (phase-separated) region 1 + 2 which exists at $c_1 < c < c_2$.

Third, we performed the calculations of temperature dependences of c, E, C_v, η, and χ at fixed chemical potential. These curves allow to determine phase transition points T_c from anomalies in energy and peaks of specific heat C_v and susceptibility χ as well as from the behavior of the order parameter η. As a result, the $c(T)$ dependence with determined the T_c value at fixed μ provide us with one point in the (c, T) phase diagram. Changing μ we obtain the set of $c(T)$ curves, i.e., the complete phase diagram of the system. Finally, to monitor the mutual orientation of ordering molecules, our calculations are supplemented by snapshots of corresponding phases at different values of c, μ, and T.

Further, temperature, chemical potential, and interactions are normalized to ε_1.

III. RESULTS OF THE NEAREST NEIGHBOR MODEL

A. Ground State Calculations and $c(\mu)$ Dependences.

Preliminary ground state calculations of phases, which might be expected in the phase diagram of model 1, show that the honeycomb phase (Figure 2a) with stoichiometric concentration c = 0.67 has the energy $E_{NN}^{hon} = 2(-3\varepsilon_1 + \mu)/3$. At the same time there are three phases candidates to exist at c = 1. These are the zigzag, the frustrated honeycomb, and the frustrated structure. The ground state energy of all these phases is the same, $E_{NN}^{zig} = E_{NN}^{frhon} = E_{NN}^{fru} = -2(\varepsilon_1 + \varepsilon_2 + \varepsilon_3) + \mu$.

It should be noted that at c = 1 our model reaches the so-called Ising limit; i.e., the s_i = 0 state vanishes and our three-state model gets to be equivalent to the two-state model. At c = 1 and $\varepsilon_1 \gg \varepsilon_2, \varepsilon_3$, model 1 is similar to the antiferromagnetic NN Ising model on triangular lattice with NN interaction ε_1. The most characteristic feature of this model is the occurrence of the frustrated phase at low temperature. The frustrated phase is the structure which cannot show the antiferromagnetic order due to limitations of the triangular lattice. As a result, this phase is configurationally distorted and, though it has its own specific order, it nevertheless is reminiscent of the disordered phase. Thus, the configurational entropy of the frustrated phase should be quite large.

The frustrated honeycomb (fhon) phase[32] has three sublattices and is an extension of the ordinary honeycomb structure, because two sublattices are orderly occupied by molecules of different states as in the honeycomb phase, but the third sublattice, while empty at c = 0.67, at c = 1 is randomly filled with molecules of both orientations (Figure 2b). This frustration leads to remnant entropy in the third sublattice only, and therefore the entropy of the fhon phase should not exceed that of the frustrated phase which is frustrated in all three sublattices. In our Monte Carlo calculations at finite temperature we obtain the fhon phase only up to concentrations $c \approx 0.95$.

The zigzag or stripe structure (Figure 2c) is the ordered phase and therefore should have the lowest entropy. It is characterized by alternating stripes of molecules in state +1 and −1. This structure has been observed in self-assembly of TMA molecules on graphite using sonication,[15] the technique which enabled to pack the structure up to maximum density.

Therefore simple ground state calculation and qualitative evaluation of configurational entropy ($S_{fr} > S_{fhon} > S_{zigzag}$) allows to predict the frustrated phase to occur on the phase diagram at c = 1, if no other interactions are included in model 1.

We started the study of thermodynamic properties calculating the $c(\mu)$ dependence at fixed values of temperature and different values of $\varepsilon_2 = \varepsilon_3$. The results given in Figure 3 show two distinct steps which correspond to two ordered phases, the honeycomb phase at c = 0.67 and the frustrated phase at full occupancy, c = 1. We also observe the discontinuity in $c(\mu)$

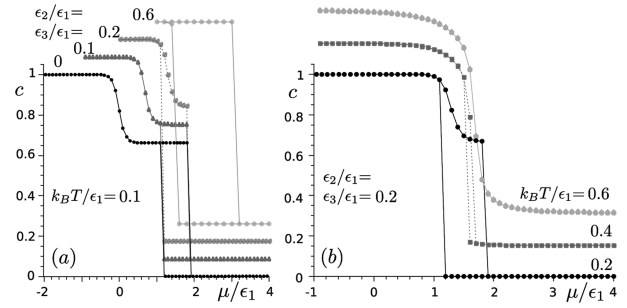

Figure 3. Concentration as a function of chemical potential: (a) for fixed k_BT/ε_1 = 0.1 and different values of $\varepsilon_2/\varepsilon_1$ and (b) for fixed $\varepsilon_2/\varepsilon_1 = \varepsilon_3/\varepsilon_1$ = 0.2 and different values of temperature. The curves, except the first, are shifted for clarity only along the vertical axis. Note the shortening and vanishing of the c = 0.67 step with increase of $\varepsilon_2/\varepsilon_1 = \varepsilon_3/\varepsilon_1$.

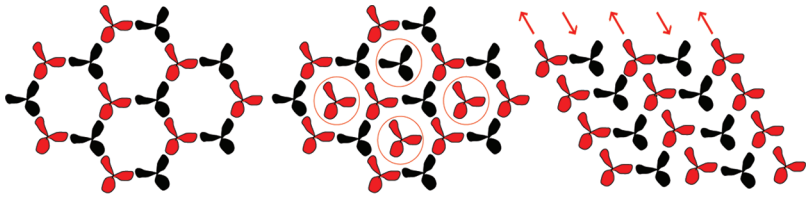

Figure 2. Schematical drawing of (a) honeycomb, (b) frustrated honeycomb, and (c) zigzag structures on NN sites of triangular lattice. Two orientations of a molecule are distinguished by gray (red in electronic version) and black colors. Arrows in (c) denote orientations on two sublattices of the zigzag phase. The circle in (b) marks the sites of third (frustrated) sublattice occupied in random.

dx.doi.org/10.1021/jp206181p | J. Phys. Chem. B 2012, 116, 2472−2482

dependence up to $c = 0.67$ which shows that at low temperature and concentration $c < 0.67$ a large two-phase (honeycomb + gas) region persists up to $c = 0$. It should be also noted that large hysteresis in chemical potential is found in $c(\mu)$ dependence, the hysteresis which defines the stability limits of the honeycomb and gas phases close to the critical value of chemical potential, $\mu_c^{\text{gas-hon}}$.

It is also seen from Figure 3a that the existence of the honeycomb phase depends on $\varepsilon_2 = \varepsilon_3$ value and temperature. This phase shrinks with increase of $\varepsilon_2/\varepsilon_1 = \varepsilon_3/\varepsilon_1$ and ceases to exist when this ratio exceeds 0.25. The step in $c(\mu)$ associated with the honeycomb phase also vanishes with increase of temperature at the honeycomb-to-gas transition point. This is demonstrated in Figure 3b.

B. Phase Diagrams at $\varepsilon_2 = \varepsilon_3 = 0$. Calculating temperature dependences of parameters characterizing the phase transition point as well as $c(\mu)$ dependences at different T values, we obtained the phase diagrams of model 1 in (c, T) and (μ, T) coordinates (Figure 4). In the (c, T) diagram the curves of fixed chemical potential, $\mu(c, T) = \text{const}$, demonstrate jumps at low values of concentration and anomalies at $c > 0.67$. Corresponding peaks in temperature dependences of specific heat or susceptibility mark the phase transitions from the gas phase to (i) honeycomb + gas two-phase region ($c > 0.67$), (ii) pure honeycomb phase ($c \approx 0.67$), (iii) fhon phase ($c > 0.67$), and (iv) frustrated structure (high-packing region, $\mu < 0$, $c \to 1$).

At low temperature the limits of existence of the honeycomb and fhon phases on the (μ, T) diagram are defined by their transitions to neighboring gas and frustrated phases. The transition between the honeycomb ($T = 0$) or fhon ($T > 0$) and frustrated phase is at $\mu_c^{\text{gas-frust}} = 0$. The first-order transition between the honeycomb and gas phase takes place at another limit, in between the interval $1.5 < \mu/\varepsilon_1 < 3$, with huge hysteresis in μ which decreases with increase of temperature. This discontinuity in $c(\mu)$ dependence leads to phase separation of the gas and honeycomb phases and occurrence of the two-phase, honeycomb + gas, region on the (c, T) phase diagram in between $c = 0$ and $c = 0.67$ at low values of temperature. With increase of T, this region decreases. The snapshots of molecular structure in the honeycomb + gas region at $c < 0.67$ and in frustrated honeycomb structure at $c > 0.67$ are presented in Figure 5.

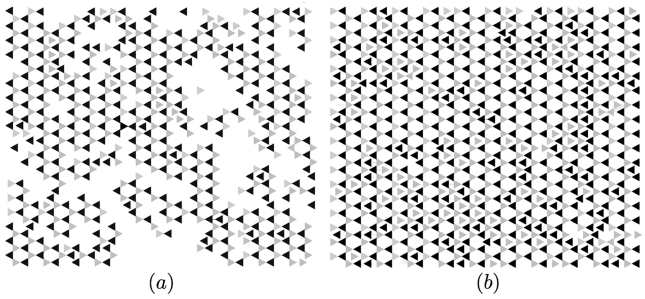

Figure 5. Snapshots at $\varepsilon_2 = \varepsilon_3 = 0$ of (a) ordering in the honeycomb + gas region at $\mu/\varepsilon_1 = 1.46$ and $k_BT/\varepsilon_1 = 0.46$ and (b) frustrated honeycomb structure at $\mu/\varepsilon_1 = 0.5$ and $k_BT/\varepsilon_1 = 0.4$. Two orientations of molecules are shown by black and gray triangles.

At low values of $\mu \gtrsim 0$ (close to the Ising limit and frustrated phase), the pure honeycomb phase is reached via fhon structure from concentration as high as $c \approx 0.95$ (e.g, $c = 0.94$ at $k_BT/\varepsilon_1 = 0.3$ when $\mu/\varepsilon_1 = 0.1$). The temperature dependences of specific heat have two peaks at $0 < \mu/\varepsilon_1 < 0.5$ (Figure 6). The peak at higher temperature is the signature of the gas-to-fhon transition. The small peak at very low values of temperature indicates an abrupt decrease of molecules in third, frustrated, sublattice and the establishing of pure ground state honeycomb structure. At $\mu/\varepsilon_1 > 0.5$, only one peak in temperature dependences of specific heat and susceptibility is found related to gas-to-fhon transition. The fhon structure exists only at $T \neq 0$.

It should be noted that the symmetry of the fhon phase is the same as that of the pure honeycomb structure. Therefore, despite the occurrence of the peak, we do not expect a real phase transition between the honeycomb and fhon phases. We also do not discard the possible interpretation of these two phases being actually one phase existing from $c = 0.67$ up to concentrations as high as 0.9–0.95.

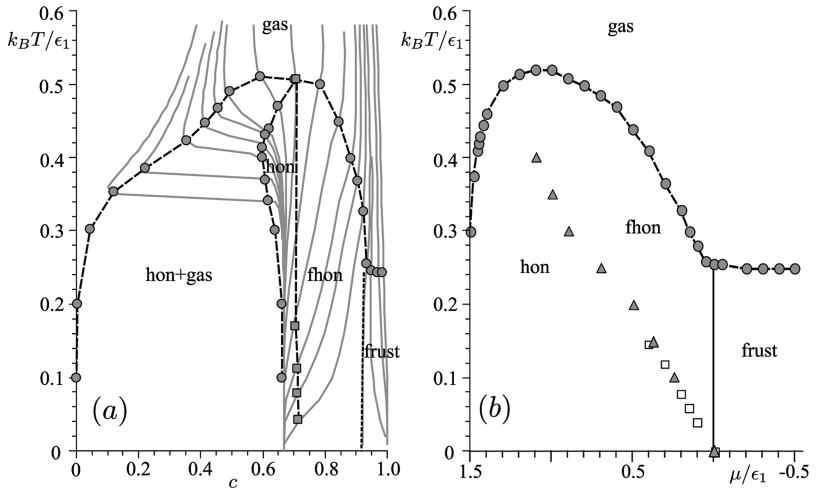

Figure 4. (a) Phase (c, T) diagram at $\varepsilon_2 = \varepsilon_3 = 0$. The constant $\mu(c, T)/\varepsilon_1$ curves (gray) are obtained at (from right to left): −0.4, −0.2, −0.05, and 0 (frust–fhon boundary), 0.1, 0.2, 0.3, 0.5, 0.8, 1.1, 1.3, 1.4, 1.42, 1.44, 1.46, 1.48, and 1.5. Phase transition points (gray circles) are the location of the specific heat maximum in $C_V(T)$ dependences. Some data points denoting the width of hon + gas phase at low temperature were taken from the magnitude of discontinuity of $c(\mu)$ dependence. Gray squares denote the location of the second, low-temperature, C_V maximum. (b) (μ, T) phase diagram. The data points separating sister structures, hon and fhon, were obtained from low-temperature C_V maximum (squares) and variation of the $c = 0.67$ step in the $c(\mu)$ dependence with temperature (triangles).

dx.doi.org/10.1021/jp206181p | J. Phys. Chem. B 2012, 116, 2472–2482

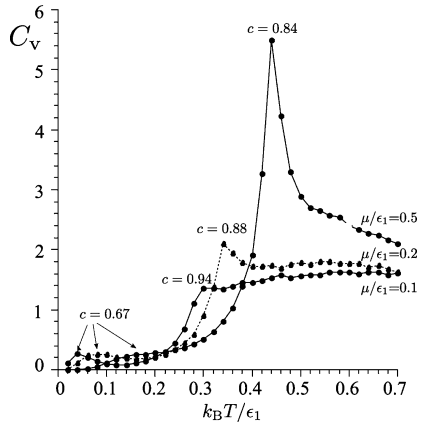

Figure 6. Temperature dependence of specific heat for $\mu/\varepsilon_1 = 0.5$, 0.2, and 0.1. Between the peaks the fhon structure is found. Perfect honeycomb structure ($c = 0.67$) is below the low-temperature peak. Numbers near peaks demonstrate the concentration of frustrated honeycomb structure at the peak temperature.

C. Increasing $\varepsilon_2 = \varepsilon_3$. With increase of $\varepsilon_2 = \varepsilon_3 > 0$, the stability limits of the honeycomb phase decrease. The transition temperature to the fhon phase also decreases as is seen from the peaks of specific heat. In general, the region of existence of the honeycomb phase shrinks in the (μ, T) diagram (see Figures 3 and 7).

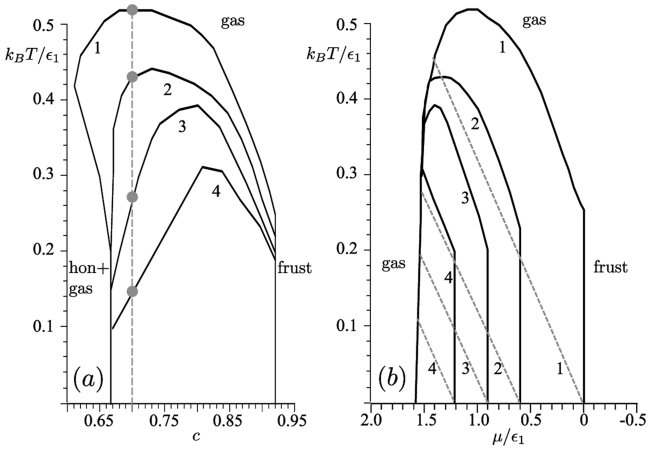

Figure 7. Shrinking of the honeycomb and frustrated honeycomb phase with increase of $\varepsilon_2 = \varepsilon_3$: (a) ($c$, T) diagram, (b) (μ, T) diagram. Only the "bell-shaped" central part enveloping these two structures is shown in both diagrams by black solid curves. Denotations of curves are 1 for $\varepsilon_2/\varepsilon_1 = 0$, 2−0.1, 3−0.15, and 4−0.2. The gray dashed lines separate frustrated honeycomb from pure honeycomb structure for the same four values of $\varepsilon_2/\varepsilon_1$. In the ($c$, T) diagram (a) the pure honeycomb structure is found up to the intersection of each curve with gray dashed line at $c \approx 0.7$.

The shrinking of the honeycomb phase is caused by expansion of the frustrated phase region. The ground state energy of the honeycomb phase does not depend on ε_2 and ε_3, i.e., $E_{hon} = 2/3(-3\varepsilon_1 + \mu)$, contrary to that of the frustrated phase: $E_{frus} = -2(\varepsilon_1 + \varepsilon_2 + \varepsilon_3) + \mu$. Therefore, the value of the critical chemical potential between these two phases depends on ε_2 and $\varepsilon_3 > 0$ only, and $\mu_c^{hon-frust} = 6(\varepsilon_2 + \varepsilon_3)$. At $\varepsilon_2 = \varepsilon_3 > 0.25\varepsilon_1$, the honeycomb phase vanishes and there is a huge two-phase, gas + frustrated, region on the (c, T) diagram between $c = 0$ and 1. Note also that for interaction values $\varepsilon_2/\varepsilon_1 = \varepsilon_3/\varepsilon_1 < 0.25$ the limits of hysteresis are approximately the same ($1.1 \lesssim \mu/\varepsilon_1 \lesssim 1.9$). For higher values of $\varepsilon_2/\varepsilon_1 = \varepsilon_3/\varepsilon_1$, when the honeycomb phase disappears and the two-phase region (gas + frustrated) dominates the phase diagram, the limits of hysteresis expand (see the $\varepsilon_2/\varepsilon_1 = \varepsilon_3/\varepsilon_1 = 0.6$ curve in Figure 3a).

It should be noted that the peak of specific heat at low temperature related to the fhon-to-hon "transition" increases with increase of $\varepsilon_2 = \varepsilon_3 > 0$ and at sufficiently high values becomes even higher than the main peak of the gas-to-fhon transition.

Separate variation of ε_2 and ε_3 shows that their effect upon the phase diagram is slightly different. Both constants of interaction enter the ground state energy of the frustrated phase with the same weight, and therefore their effect on a location of the frustrated-to-honeycomb phase transition is similar. The difference is seen mostly in the gas-to-fhon (smaller ε_2 and ε_3) or gas-to-mixed phase (larger ε_2 and ε_3) transition temperature. In Figure 8 the fragments of the (c, T) diagram at exactly the same values of μ are presented for $\varepsilon_2 = 0$ and $\varepsilon_3/\varepsilon_1 = 0.2$ and $\varepsilon_2/\varepsilon_1 = 0.2$ and $\varepsilon_3 = 0$ (a) and $\varepsilon_2 = 0$ and $\varepsilon_3/\varepsilon_1 = 0.4$ and $\varepsilon_2/\varepsilon_1 = 0.4$ and $\varepsilon_3 = 0$ (b). For $\varepsilon_2 > \varepsilon_3$ the transition temperatures are higher compared to those of $\varepsilon_2 < \varepsilon_3$.

In case (a) the phase diagram undergoes some quantitative, but not qualitative, changes in comparison to the phase diagram in Figure 4. In case (b) the changes are important: the region of the frustrated honeycomb phase is rather small, and only traces of the pure honeycomb structure are left at low temperature.

IV. NEAREST AND NEXT-NEAREST NEIGHBOR MODEL: ZIGZAG OR FRUSTRATED PHASE

In all presented phase diagrams, the frustrated phase occurs at $c \to 1$, although there are no reports of this structure being observed in molecular self-assemblies of triangular-shaped molecules. One reason for this discrepancy is clear: in contrast to real systems, in our numerical experiment the molecules cannot avoid the frustration because they move only over NN sites of rescaled triangular lattice (Figure 1c). Moreover, we restricted our model 1 by strong, but comparatively short-range, H-bondings, i.e., NN interactions. At the same time, our ground state calculations of the NN model demonstrated that the frustrated phase has a very small advantage of higher entropy compared with other structures which might be obtained at $c = 1$. Therefore the frustrated phase might be substituted by another structure, if additional longer-range contributions are expected, e.g., of dipole−dipole[29] or elastic (coming from deformation of substrate by molecules)[52] origin. Longer-range adsorbate−adsorbate interactions were observed recently for antraquinone forming an unusual type of a H-bonded honeycomb structure on Cu(111).[7,46]

Specifically for TMA molecules, the dipole interactions could be ruled out, and at the moment we have no evidence which would support the presence of elastic interactions. Still, not completely discarding the possibility of elastic deformations, we assume that there might be additional *indirect* next-nearest neighbor (NNN) interactions via long-tail solvent acid molecules which occupy the cavities between the TMA molecules. These solvent molecules are not seen in experiments due to their low stabilization energy and short residence time. Some idea about their location might be gained from supplementary files of ref 16 where the ball-and-stick model of the honeycomb structure of BTB molecules on graphite with coadsorbed nonanoic acid solvent molecules is given. Irrespective of the real position of the solvent molecules, it is clear that the indirect part (via solvents) of NN intermolecular interactions is negligible compared with

dx.doi.org/10.1021/jp206181p | J. Phys. Chem. B 2012, 116, 2472−2482

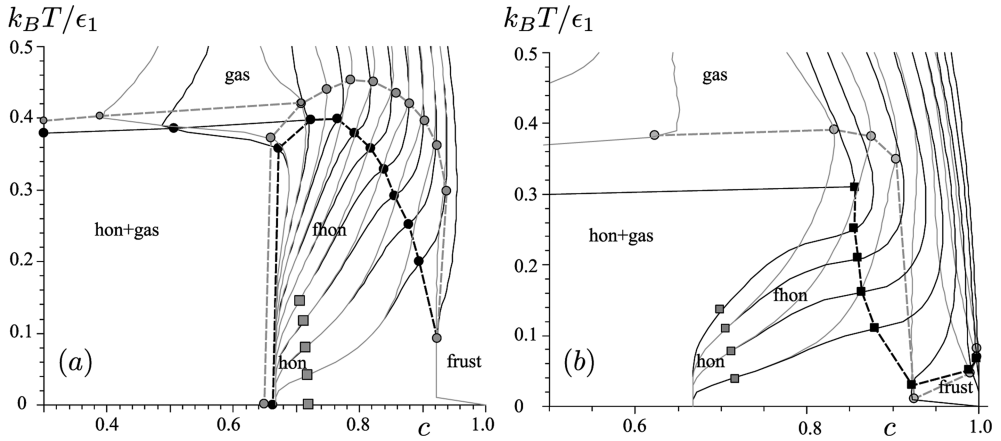

Figure 8. Fragments of the (c, T) diagram for (a) $\varepsilon_2/\varepsilon_1 = 0$; $\varepsilon_3/\varepsilon_1 = 0.2$ (black curves) and $\varepsilon_2/\varepsilon_1 = 0.2$; $\varepsilon_3/\varepsilon_1 = 0$ (gray curves) and (b) $\varepsilon_2/\varepsilon_1 = 0$; $\varepsilon_3/\varepsilon_1 = 0.4$ (black curves) and $\varepsilon_2/\varepsilon_1 = 0.4$; $\varepsilon_3/\varepsilon_1 = 0$ (gray curves). The black and gray curves are obtained for the same fixed μ values. In (a) μ/ε_1 is equal to (from right to left) 1.5, 1.4, 1.3, 1.2, 1.1, 1.0, 0.9, 0.8, 0.7, and 0.6. In (b) $\mu/\varepsilon_1 = 1.62$, 1.59, 1.5, 1.4, 1.3, 1.2, 1.1, 1.0, 0.9, and 0.8. The black and gray symbols correspond to peaks of specific heat for black and gray curves, respectively. The gray rectangles denote the peaks of specific heat for pure honeycomb phase. They have the same value for black and gray curves.

dimeric H-bonding interaction ε_1. But the NNN interaction ε_4 (Figure 9), which must be much smaller than ε_1, can be entirely

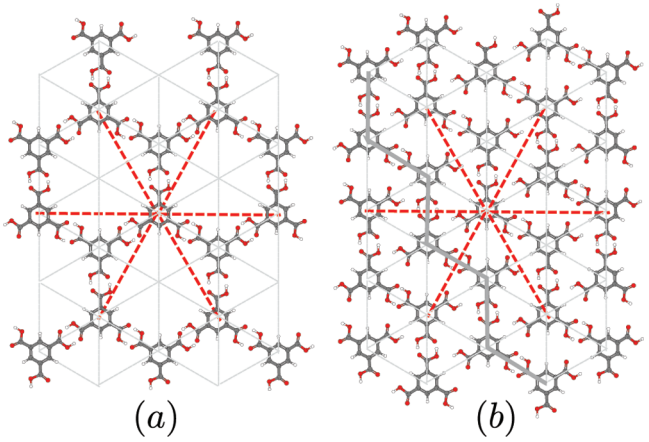

Figure 9. NNN interactions in (a) honeycomb and (b) zigzag TMA structure. Gray (red in electronic version) dashed lines mark the NNN interactions of the central molecule. Gray thicker line in (b) depicts the zigzag arrangement of H-bonded molecules.

caused by the indirect interaction via solvent molecules. Moreover, the NNN intermolecular interaction between molecules of the same state (orientation), $\varepsilon_4^{\ll}$, might be different from that between the molecules of different states (orientations), $\varepsilon_4^{><}$, since the change of orientation of the TMA molecule might change the positions of solvent molecules in between and correspondingly might lead from attraction to repulsion.

It is known from statistical modeling of Ising-type lattice systems that antiferromagnetic NNN pair[53,54] or three-body trio in a line interaction[55] might be responsible for the occurrence of the phases with characteristic zigzag (stripe) pattern.

Here we just assume that two molecules in the NNN sites attract each other by ε_4, if their orientations are different ($\varepsilon_4^{><} = -\varepsilon_4$), and repulse each other by ε_4, if their orientations are the same ($\varepsilon_4^{\ll} = \varepsilon_4$). Therefore, to compare with the energy of the NN model, the ground state energy of the honeycomb phase increases, the energy of the zigzag phase decreases, and the energy of the frustrated phase stays on average unchanged (see also Figure 9)

$$E^{\text{hon}} = E_{\text{NN}}^{\text{hon}} + 2/3(6\varepsilon_4^{<<}) = E_{\text{NN}}^{\text{hon}} + 4\varepsilon_4 \quad (3)$$

$$E^{\text{zig}} = E_{\text{NN}}^{\text{zig}} + 2\varepsilon_4^{<<} + 4\varepsilon_4^{><} = E_{\text{NN}}^{\text{zig}} - 2\varepsilon_4$$

$$E^{\text{fru}} = E_{\text{NN}}^{\text{fru}} + 3\varepsilon_4^{<<} + 3\varepsilon_4^{><} = E_{\text{NN}}^{\text{fru}}$$

Since $E_{\text{NN}}^{\text{zig}} = E_{\text{NN}}^{\text{fru}}$, the zigzag phase is expected to exist at full occupancy. We do not use bond vector formalism for the NNN interactions, because they are clearly indirect. It should be noted that the results would not essentially change, if both NNN interactions, $\varepsilon_4^{><}$ and $\varepsilon_4^{\ll}$, were attractive and $|\varepsilon_4^{><}| > |\varepsilon_4^{\ll}|$.

We performed the calculations of the phase diagrams and $c(\mu)$ dependences at different values of increasing ε_4. A very small value of $\varepsilon_4/\varepsilon_1 < 0.02$ does not change the phase diagrams much, except for the obvious fact that the frustrated phase is substituted by the zigzag structure. The transition from the honeycomb or frustrated honeycomb phase to zigzag phase is still continuous. Taking this into account, the phase diagrams at $\varepsilon_4/\varepsilon_1 = 0.01$ might be well represented by Figure 4 with a little bit lower transition temperature to the honeycomb phase. With further increase of ε_4 the phase diagrams and $c(\mu)$ dependences start to change, the main difference being the abrupt jump of concentration between the steps at $c = 0.67$ and $c = 1$ in $c(\mu)$ dependence and, as a result, the occurrence of the two-phase region, hon + zigzag, on the phase diagram (see Figures 10 and 11). The discontinuity is most likely related to different symmetry of threefold honeycomb and stripe-type zigzag phases. With increase of ε_4 and at low temperature, the hysteresis between the steps at $c = 0.67$ and $c = 1$ increases, and the region of μ, where the honeycomb phase exists, decreases (Figure 10a). With decrease and shrinking of the honeycomb phase, the hysteresis between the step $c = 0$ (gas phase) and $c = 0.67$ (honeycomb phase) correspondingly decreases. The honeycomb phase completely decomposes at $\varepsilon_4/\varepsilon_1 > 0.15$. Another interesting aspect is the decrease of transition temperature with increase of NNN interactions. As the honeycomb phase shrinks with increase of ε_4, so does the gas-to-honeycomb (or gas-to-frustrated honeycomb) phase transition temperature T_c: if the bell-shaped maximum in Figure 4 is at $k_BT_c/\varepsilon_1 = 0.5$, it is at 0.25 in Figure 11 ($\varepsilon_4/\varepsilon_1 = 0.1$). At even higher values of

dx.doi.org/10.1021/jp206181p | J. Phys. Chem. B 2012, 116, 2472–2482

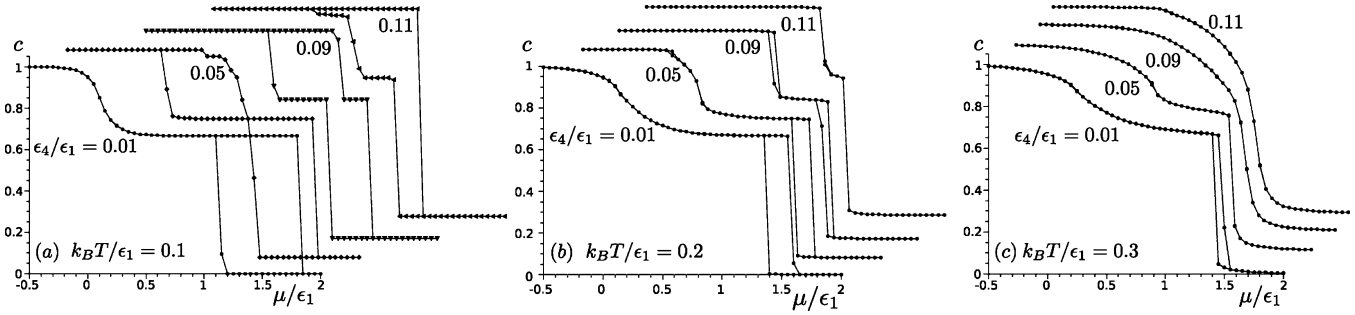

Figure 10. $c(\mu)$ dependence for different values of $\varepsilon_4/\varepsilon_1$ at k_BT/ε_1 = 0.1 (a), 0.2 (b), and 0.3 (c). All the curves, except the first one, are shifted for convenience, and their limits are between 0 and 1 in a concentration and between −0.5 and 2 in a chemical potential scale.

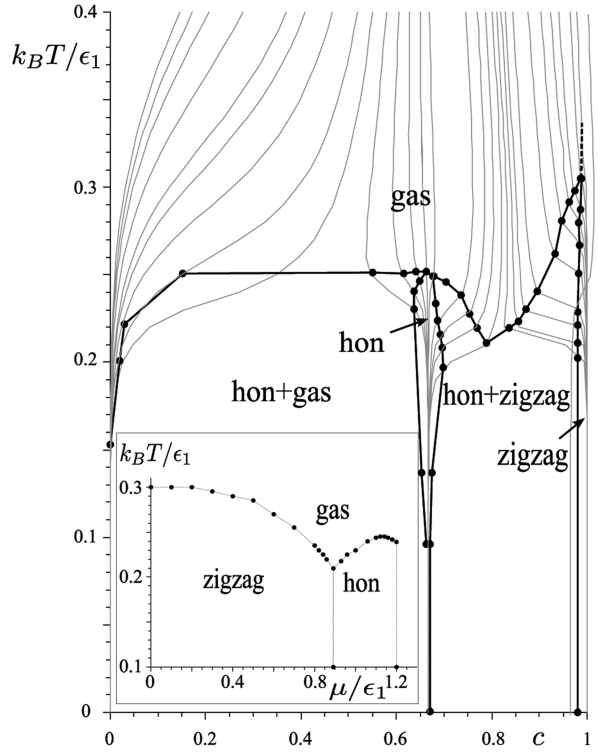

Figure 11. Phase diagram with zigzag phase in (c, T) and (μ, T) (inset) coordinates at $\varepsilon_2 = \varepsilon_3 = 0$ and $\varepsilon_4/\varepsilon_1 = 0.1$. Other denotations as in Figure 4. The $\mu(c, T)/\varepsilon_1$ = const curves are obtained at (from right to left): 0, 0.2, 0.4, 0.5, 0.6, 0.7, 0.8, 0.84, 0.86, 0.88 (zigzag−hon boundary), 0.9, 0.93, 0.96, 1.0, 1.06, 1.1, 1.12, 1.14, 1.16, 1.18 (hon−gas boundary), 1.2, 1.22, 1.25, 1.28, 1.3, 1.35, 1.4, 1.43, and 1.46.

$\varepsilon_4/\varepsilon_1 > 0.15$, when the $c = 0.67$ step in the $c(\mu)$ dependence and the honeycomb phase vanish, all the interval of concentration values between 0 and 1 in the phase diagram is occupied by the two-phase region, gas + zigzag phase.

In Figure 11 we demonstrate the phase diagrams obtained at $\varepsilon_4/\varepsilon_1 = 0.1$. The region between $c = 0.67$ and $c = 1$ is occupied by two-phase, honeycomb + zigzag, structure. A very interesting feature of the phase diagram is observed in temperature limits between 0.2 and 0.3, where with increase of concentration the sequence of phase transitions, honeycomb → honeycomb + zigzag → gas → honeycomb + zigzag → zigzag, is found. The last transition, as a small concentration jump decreasing with increase of temperature, might be seen in Figure 12 at k_BT/ε_1 = 0.21, 0.24, and 0.27 and concentration between 0.8 and 1. The curve at k_BT/ε_1 = 0.24 demonstrates all the sequence of phase

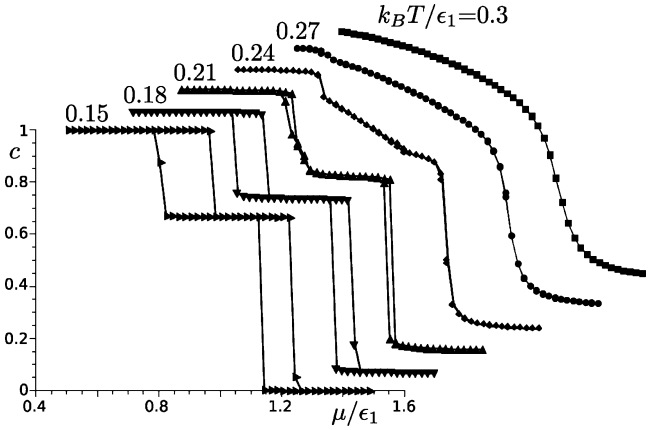

Figure 12. $c(\mu)$ dependence at $\varepsilon_4/\varepsilon_1$ = 0.1 for different values of temperature. All the curves, except the first one, are shifted for convenience, and their limits are between 0 and 1 in a concentration and between 0.5 and 1.5 in a chemical potential scale.

transitions with long interval of linear $c(\mu)$ dependence (corresponding to gas phase) at $0.7 \lesssim c \lesssim 0.85$. The gradual formation of a zigzag structure, starting in a two-phase region and ending with almost perfect zigzag phase, is presented in snapshots of Figure 13.

V. DISCUSSION

The results of our modeling demonstrate the limits of the honeycomb phase existence in a system of triangular molecules with strongly interacting vertices. In a model with three main interactions, i.e., the model which is appropriate for the self-assemblies of TMA and similar H-bonded molecules, the honeycomb structure represents the system of molecules coupled by the main "tip-to-tip" interaction and, at the same time, affected by two remaining interactions. We have shown that the effect of these two interactions might be crucial for existence of the honeycomb phase, and the structure might even vanish from the phase diagram. Since the substrate affects H-bonding of TMA molecules, this could, at least, partly explain why the honeycomb structure found on graphite,[8,10,12,18,23] Au(111),[19−21] and Cu(100)[22] is not found on some other surfaces, e.g., Si(7 × 7)[35] and Cu(110).[14]

The effect of remaining interactions manifests itself also in decrease of the transition temperature to the honeycomb phase. This result shows how quite realistic values of disordering temperature for the honeycomb phase of TMA might be obtained. Consider first the values of interaction constants obtained in other calculations. The value of the main dimeric attractive

dx.doi.org/10.1021/jp206181p | J. Phys. Chem. B 2012, 116, 2472−2482

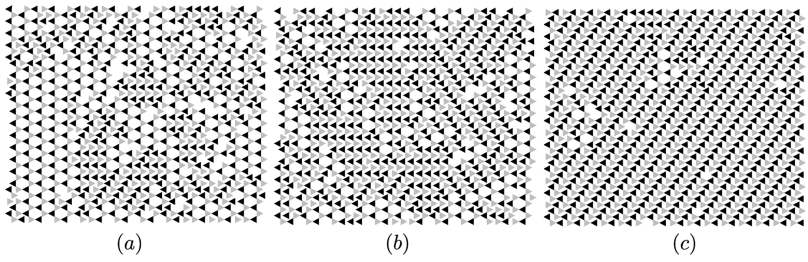

Figure 13. Snapshots in two-phase honeycomb−zigzag region just below the phase transition point (a) $k_BT/\varepsilon_1 = 0.21$, $c = 0.8$ and (b) $k_BT/\varepsilon_1 = 0.24$, $c = 0.89$. (c) Snapshot of zigzag phase at $k_BT/\varepsilon_1 = 0.23$, $c = 0.98$. Two orientations of molecules are shown by black and gray triangles.

interaction constant ε_1 was determined by the DFT calculations in gas phase ($\varepsilon_1 = -20.4$ kcal/mol[10]) and the pseudopotential MOPAC calculations for close-packed zigzag structure on graphite ($\varepsilon_1 = -32$ to -35 kcal/mol[15]). In this MOPAC calculation also the value of $\varepsilon_3 = -9.5$ to -9.8 kcal/mol was obtained and presumably ε_2 was estimated as much smaller. To obtain the estimate of ε_2, we also analyzed the results for alcohol-connected TMA tapes,[10] where the interaction energies of three four-molecule blocks in gas phase were calculated by the DFT. Although in a slightly deformed form, these blocks possess all three interactions ε_1, ε_2, and ε_3 as well as the TMA−water interaction. Taking into account the value of dimeric interaction in the gas phase ($\varepsilon_1 = -20.4$ kcal/mol[10]), the $\varepsilon_2 \approx -7$ kcal/mol can be estimated from a system of three linear equations. Note, however, that this interaction is deformed to accommodate one H-bond. All these results imply that ε_2 and ε_3 make quite an important contribution and their magnitude might constitute 20−30% of the main dimeric interaction constant. Our calculations of phase diagram in Figure 4 demonstrate that even in the absence of ε_2 and ε_3 interactions the phase transition temperature k_BT/ε_1 to pure honeycomb phase might also be very low, even of the order of 0.01, e.g., 0.04−0.08 (when $\mu/\varepsilon_1 = 0.1-0.2$) corresponding to 400−800 K. However such "realistic" values of temperature can be obtained only in a very tiny interval of values of chemical potential almost corresponding to honeycomb-to-frustrated (or to-zigzag) phase boundary, $\mu \to 0$. But when the ratio of interactions $\varepsilon_2/\varepsilon_1 \sim \varepsilon_3/\varepsilon_1$ increases up to 0.2−0.3, the transition temperature to pure honeycomb structure is realistic for *any* values of μ corresponding to the honeycomb phase, because the size of the "bell" in the (μ, T) phase diagram drastically decreases, as might be seen in Figure 7.

Inclusion of the NNN pair interactions leads to domination of the stripe-type zigzag phase at close packing (Ising limit). As a result, both important experimentally found TMA structures (honeycomb and zigzag) coexist in a phase diagram. Increase of the NNN interactions have a similar effect as that of ε_2 or ε_3. It decreases the limits of existence of the honeycomb phase, reduces the phase transition temperature, and, as an extra effect, stimulates the occurrence of a two-phase structure, the honeycomb + zigzag phase.

The phase diagrams in this paper were presented in the concentration−temperature coordinates. In experiments the ordered molecular structures are usually characterized by molecular packing density, ρ. Consider how the ratio of concentrations of pure honeycomb and pure zigzag phases (0.67/1) correspond to the ratio of packing densities of the same TMA phases on graphite. The packing densities of the honeycomb and zigzag structures are equal to 0.8[12] and 1.29 mol/nm^2,[15] respectively. Thus, the ratio ρ_{hon}/ρ_{zig} is 0.62 which gives satisfactory agreement with our simple NN model. It should be also noted that $\rho_{zig} = 1.29$ mol/nm^2 was obtained by refining the STM results by MOPAC simulation. This result might be slightly overestimated, since the zigzag structure is obtained to be even denser than that of the "ideal" superflower phase, for which the same MOPAC simulation[15] gives the value equal to 1.19 mol/nm^2. It is known, however, that this structure has the densest packing of all TMA structures (e.g., 1.34 mol/nm^2 on Au(111)[21]) and due to its high density is found only in small fragments, rather than as a long-range structure. Decrease of ρ_{zig}, e.g., from 1.29 to 1.19 mol/nm^2, would provide a perfect agreement with our model.

Finally, we would like to comment on applicability of our model to ordering of the TMA molecules. The main aim of our simulation was to demonstrate the model and its main tendencies—the effect of main interaction parameters on existence of phases, in particular, rather to obtain a good agreement with experiment. In real experiment there are many more sites for TMA molecules diffusion and ordering than the simple NN model allows. At the same time a majority of these sites are eliminated due to infinite exclusion caused by the size of the molecule being much larger than the length scale of substrate distances. Part of the intersites is inevitably omitted in such a reduction of the system to the NN model. Therefore, the number of degrees of freedom decreases enhancing the tendency to order. Nevertheless, we do not think that this can qualitatively affect the obtained phase diagrams, although the transition temperature might slightly increase with respect to experimental situation.

It should be also noted that in this study we restricted ourselves to pairwise bonding schemes. It is known that the trimeric bonding might also be important for the self-assemblies of TMA molecules, and it is quite possible that three-molecule interactions must be taken into account in order to describe the so-called flower or superflower structures.

APPENDIX A: MAPPING MODEL 1 TO KNOWN THREE-STATE ANTIFERROMAGNETIC MODELS

Compared to magnetism models, three binding schemes of Figure 1a might be interpreted as two antiferromagnetic (AFM) interactions, ε_1 and ε_2, between molecules in different orientations and ferromagnetic (FM) interaction, ε_3, between molecules of the same orientation. The fact that there might be two different AFM interactions makes an important difference in ordering of triangular molecules from those of spins, atoms, or binary alloys, i.e., the systems which might be described by the two-state orientational ($\sigma_i = \pm 1$) or occupational variables ($n_i = 1, 0$). There is no difference in interaction direction for antiferromagnetically interacting pair of spins in the Ising model ($v(+,-) = v(-,+)$) or different point atoms A and B in binary alloy, $v(AB) = v(BA)$. As is seen from Figure 1c, this does not apply to TMA molecules. Only two molecules coupled by FM

dx.doi.org/10.1021/jp206181p | J. Phys. Chem. B 2012, 116, 2472−2482

interaction ε_3 could be ascribed the same energy as for the Ising model, (+, +) and (−, −). However two AFM interactions are very different. In principle, it is possible to map this model to the Ising model,[39] but only for the FM case. The AFM model would give the mixture of AFM states with the energies ε_1 and ε_2 in their ground state. Thus, trying to order the triangular molecules in a honeycomb structure, i.e., the one characterized by ε_1 bonds only, makes the model more complicated than the pure AFM Ising model.

It is also interesting to compare our model with other, more familiar, statistical models, the three-state Potts model and BEG model on triangular lattice in particular. The Potts model[41] has the form

$$\mathcal{H} = -\varepsilon \sum_{i,j} \delta(s_i, s_j) \tag{A1}$$

where ε is the interaction constant which is positive for FM and negative for AFM model, $\delta(s_i, s_j)$ is Kroeneker delta function equal to 1 when the states in NN sites i and j are the same and zero otherwise. Here s_i is the Potts variable at site i which is associated with state values +1, −1, and 0. The two-state Potts model is equivalent to the Ising model. On a tripartite lattice, the three-state AFM Potts model has the first-order phase transition at $T_c/\varepsilon = 0.627$.[56] This transition changes to the structure in which first and second sublattices are occupied with molecules in state +1 and −1 respectively and the third sublattice is empty (state 0). In our model this is equivalent to the transition to occupational (but not orientational) honeycomb structure which we further call geometrical honeycomb (ghon). For triangular molecules this structure has the features of both AFM bonding schemes, ε_1 and ε_2, shown in Figure 1a. Thus, we cannot obtain full correspondence with the three-state AFM Potts model for pure honeycomb phase binded by the interaction ε_1, but we can map a simplified version of our model when $\varepsilon_1 = \varepsilon_2$.

Consider the honeycomb structure, where the central molecule in orientation +1 is surrounded at the NN sites by three molecules in a state −1 and three vacancies in a state 0 in alternating order. Calculate the energy difference by changing the state of the central molecule from +1 to −1 (rotation) and from +1 to 0 (removal) and compare the results for our and the three-state AFM Potts model. The initial energy of the central molecule in a three-state AFM Potts model would be zero. In our model this energy would be either $-3\varepsilon_1$ or $-3\varepsilon_2$, depending on a bonding scheme ($\alpha = 1$ or -1) of surrounding molecules. Since $\varepsilon_1 = \varepsilon_2$, it does not matter. The energy of the AFM Potts model after rotation and removal of the central molecule is the same, 3ε. Changing the state of the central molecule in our model gives the final energy $-3\varepsilon_3$ and $-\mu$ for rotation and removal, respectively. Comparing the energy difference for the Potts and our model, we obtain the following: $\varepsilon = \varepsilon_1 - \varepsilon_3$ and $\mu = 3\varepsilon_3$.

Considering this result and comparing the model energies in Table A1, it is seen that our model might be mapped to the three-state AFM Potts model at negative values of ε_3 which correspond to repulsion of FM state. The geometric honeycomb structure might be found at negative values of μ when $-6(|\varepsilon_3| - \varepsilon_1) < \mu < 0$. Outside this interval the phase is surrounded by the frustrated and gas phases.

Now, compare our model and the BEG model[42,43] which has the energy

$$\mathcal{H} = -J \sum_{i,j} s_i s_j - K \sum_{i,j} s_i^2 s_j^2 + \mu \sum_i s_i^2 \tag{A2}$$

Table A1. Comparison of Interactions and Interaction Energy of "Geometrical" Honeycomb Phase on Triangular Lattice in Our Model, Three-State AFM and FM Potts, and BEG Models

interactions	our model	AFM (FM) Potts model	BEG model
+1 + 1, −1 − 1	$-\varepsilon_3$	$+\varepsilon$ ($-\varepsilon$)	$-J - K$
+1 − 1, −1 + 1	$-\varepsilon_1$ or $-\varepsilon_2$	0	$+J - K$
±1 0, 0 ± 1	0	0	0
0 0	0	$+\varepsilon$ ($-\varepsilon$)	0
interaction energy of ghon phase (per spin)	$-2\varepsilon_1 + 2/3\ \mu$, $\varepsilon_1 = \varepsilon_2$	0	$+2J - 2K + 2/3\ \mu$

where interactions J and K characterize orientational and occupational ordering, respectively. Thus, $J > 0$ corresponds to FM and $J < 0$ to AFM BEG model. Performing the same calculation for rotation and creation of a vacancy in a honeycomb phase as has been already done for the AFM Potts model, we obtain $\varepsilon_1 = \varepsilon_2 = -J + K$ and $\varepsilon_3 = J + K$ as mapping conditions of our and the BEG model. It should be noted that they demonstrate that the FM and AFM interactions can, in principle, have the same sign if they comprise orientational and occupational parts of different magnitude.

AUTHOR INFORMATION

Corresponding Author

*E-mail: et@et.pfi.lt.

ACKNOWLEDGMENTS

We are grateful to V. Petrauskas, I. Šimkienė, and S. Lapinskas for a number of valuable discussions.

REFERENCES

(1) Huang, Y. L.; Chen, W; Li, H.; Ma, J; Pflaum, J.; Wee, A. T. S. *Small* **2010**, *6*, 70.
(2) Barth, J. V. *Annu. Rev. Phys. Chem.* **2007**, *58*, 375.
(3) *Handbook on Nanofabrication*; Wiederrecht, P., Ed.; Elsevier: Amsterdam, The Netherlands, 2010.
(4) Yang, Y.; Wang, C. *Curr. Opin. Colloid Interface Sci.* **2009**, *14*, 135.
(5) Kind, M.; Woell, C. *Prog. Surf. Sci.* **2009**, *84*, 230.
(6) Bartels, L. *Nat. Chem.* **2010**, *2*, 87.
(7) Pawin, G.; Wong, K. L.; Kwon, K.-Y.; Bartels, L. *Science* **2006**, *313*, 961.
(8) MacLeod, J. M.; Ivasenko, O.; Perepichka, D. F.; Rosei, F. *Nanotechnology* **2007**, *18*, 424031.
(9) MacLeod, J. M.; Ivasenko, O.; Fu, C.; Taerum, T.; Rosei, F.; Perepichka, D. F. *J. Am. Chem. Soc.* **2009**, *131*, 16844.
(10) Nath, K. G.; Ivasenko, O.; MacLeod, J. M.; Miwa, J. A.; Wuest, J. D.; Nanci, A.; Perepichka, D. F.; Rosei, F. *J. Phys. Chem. C* **2007**, *111*, 16996.
(11) Ivasenko, O.; Perepichka, D. F. *Chem. Soc. Rev.* **2011**, *40*, 191.
(12) Lackinger, M.; Griessl, S.; Heckl, W. M.; Hietschold, M.; Flynn, G. W. *Langmuir* **2005**, *21*, 4984.
(13) Kampschulte, L.; Lackinger, M.; Maier, A.-K.; Kishore, R. S. K.; Griessl, S.; Schmittel, M.; Heckl, W. M. *J. Phys. Chem. B* **2006**, *110*, 10829.
(14) Classen, T.; Lingenfelder, M.; Wang, Y.; Chopra, R.; Virojanadara, C.; Starke, U.; Costantini, G.; Fratesi, G.; Fabris, S.; de Gironcoli, S.; Baroni, S.; Haq, S.; Raval, R.; Kern, T. *J. Phys. Chem. A* **2007**, *111*, 12589.
(15) Ha, N. T. N.; Gopakumar, T. G.; Gutzler, R.; Lackinger, M.; Tang, H.; Hietschold, M. *J. Phys. Chem. C* **2010**, *114*, 3531.
(16) Gutzler, R.; Sirtl, T.; Dienstmaier, J. F.; Mahata, K.; Heckl, V. M.; Schmittel, M.; Lackinger, M. *J. Am. Chem. Soc.* **2010**, *132*, 5084.

(17) Theobald, J. A.; Oxtoby, N. S.; Phillips, M. A.; Champness, N. R.; Beton, P. H. *Nature* **2003**, *424*, 1029.
(18) Nath, K. G.; Ivasenko, O.; Miwa, J. A.; Dang, H.; Wuest, J. D.; Nanci, A.; Perepichka, D. F.; Rosei, F. *J. Am. Chem. Soc.* **2006**, *128*, 4212.
(19) Su, G. J.; Zhang, H. M.; Wan, L. J.; Bai, C. L.; Wandlowski, Th. *J. Phys. Chem. B* **2004**, *108*, 1931.
(20) Li, Z.; Han, B.; Wan, L. J.; Wandlowski, Th. *Langmuir* **2005**, *21*, 6915.
(21) Ye, Y. C.; Sun, W.; Wang, Y. F.; Shao, X.; Xu, X. G.; Cheng, F.; Li, J. L.; Wu, K. J. *Phys. Chem. C* **2007**, *111*, 10138.
(22) Dmitriev, A.; Lin, N.; Weckesser, J.; Barth, J. V.; Kern, K. J. *Phys. Chem. B* **2002**, *106*, 6907.
(23) Griessl, S.; Lackinger, M.; Edelwirth, M.; Hietschold, M.; Heckl, W. M. *Single Mol.* **2002**, *3*, 25.
(24) Kampschulte, L.; Werblowsky, T. L.; Kishore, R. S. K.; Schmittel, M.; Heckl, W. M.; Lackinger, M. *J. Am. Chem. Soc.* **2008**, *130*, 8502.
(25) Silly, F.; Weber, U. K.; Shaw, A. Q.; Burlakov, V. M.; Castell, M. R.; Briggs, G. A. D.; Pettifor, D. G. *Phys. Rev. B* **2008**, *77*, 201408.
(26) Weber, U. K.; Burlakov, V. M.; Perdigao, L. M. A.; Fawcett, R. H. J.; Beton, P. H.; Champness, N. R.; Jefferson, J. H.; Briggs, G. A. D.; Pettifor, D. G. *Phys. Rev. Lett.* **2008**, *100*, 156101.
(27) Li, Y. B.; Ma, Z.; Qi, G. C.; Yang, Y. L.; Zeng, Q. D.; Fan, X. L.; Wang, C.; Huang, W. J. *Phys. Chem. C* **2008**, *112*, 8649.
(28) Gutzler, R.; Sophie, L.; Mahata, K.; Schmittel, M.; Heckl, W. M.; Lackinger, M. *Chem. Commun.* **2009**, 680.
(29) Berner, S.; de Wild, M.; Ramoino, L.; Ivan, S.; Barratoff, A.; Guentherodt, H.-J.; Suzuki, H.; Schlettwein, D.; Jung, T. A. *Phys. Rev. B* **2003**, *68*, 115410.
(30) Petrauskas, V.; Lapinskas, S.; Tornau, E. E. *J. Chem. Phys.* **2004**, *120*, 11815.
(31) Charra, F.; Cousty, J. *Phys. Rev. Lett.* **1998**, *80*, 1682.
(32) Osipov, M.; Stelzer, J. *Phys. Rev. E* **2003**, *67*, 061707.
(33) Andelman, D.; de Gennes, P.-G. *C.R. Acad. Sci., Paris* **1988**, *307*, 233.
(34) Pelizzola, A.; Pretti, M.; Scalas, E. *J. Chem. Phys.* **2000**, *112*, 8126.
(35) El Garah, M.; Makoudi, Y.; Cherioux, F.; Duverger, E.; Palmino, F. *J. Phys. Chem. C* **2010**, *114*, 4511.
(36) Pasini, P.; Chiccoli, C.; Zannoni, C. In *Advances in the Computer Simulation of Liquid Crystals*; Pasini, P., Zannoni, C., Eds.; Kluwer: Dordecht, The Netherlands, 2000; p 99.
(37) Binder, K.; Paul, W. *Macromolecules* **2008**, *41*, 4537.
(38) Higo, J.; Endo, S.; Nagayama, K. *Chem. Phys. Lett.* **1992**, *198*, 300.
(39) Šarlah, A.; Frey, E.; Franosch, T. *Phys. Rev E* **2007**, *75*, 021402; *Phys. Rev. Lett.* **2005**, *95*, 088302.
(40) Bianchi, E.; Largo, J.; Tartaglia, P.; Zaccarelli, E.; Sciortino, F. *Phys. Rev. Lett.* **2006**, *97*, 168301.
(41) Wu, F. Y. *Rev. Mod. Phys.* **1982**, *54*, 235.
(42) Blume, M.; Emery, V. J.; Griffiths, R. B. *Phys. Rev. A* **1971**, *4*, 1071.
(43) Sivardiere, J.; Lajzerowicz, J. *Phys. Rev. A* **1975**, *11*, 2090.
(44) Fortuna, S.; Cheung, D. L.; Troisi, A. *J. Phys. Chem. B* **2010**, *114*, 1849.
(45) Zhdanov, V. P. *Phys. Rev. B* **2007**, *76*, 033406.
(46) Kim, K.; Einstein, T. L. *Phys. Rev. B* **2011**, *83*, 245414.
(47) Martsinovich, N.; Troisi, A. *J. Phys. Chem. C* **2010**, *114*, 4376.
(48) Rohr, C.; Balbas Gambra, M.; Gruber, K.; Constable, E. C.; Frey, E.; Franosch, T.; Hermann, B. A. *Nano Lett.* **2010**, *10*, 833.
(49) Haran, M.; Goose, J. E.; Clote, N. P.; Clancy, P. *Langmuir* **2007**, *23*, 4897.
(50) Choudhary, D.; Clancy, P.; Shetty, R.; Escobedo, F. *Adv. Funct. Mater.* **2006**, *16*, 1768.
(51) Metropolis, N.; Rosenbluth, A. W.; Rosenbluth, M. N.; Teller, A. H; Teller, E. *J. Chem. Phys.* **1953**, *21*, 1087.
(52) Knorr, N.; Brune, H.; Epple, M.; Hirstein, A.; Schneider, M. A.; Kern, K. *Phys. Rev. B* **2002**, *65*, 115420.
(53) Fan, C.; Wu, F. Y. *Phys. Rev.* **1969**, *179*, 560.
(54) Joknys, A.; Tornau, E. E. *J. Magn. Magn. Mater.* **2009**, *321*, 137.
(55) Petrauskas, V.; Tornau, E. E. *Phys. Rev. B* **2010**, *82*, 115433.
(56) Adler, J.; Brandt, A.; Janke, W.; Shmulyian, S. *J. Phys. A* **1995**, *28*, 3117.